Room-Temperature Macroscopic Coherence of Two Electron-Hole Plasmas in a Microcavity

Qi Jie,[1] Keye Zhang,[1] Chih-Wei Lai,[2] Feng-Kuo Hsu,[2] Weiping Zhang,[3,7,8,*] Song Luo,[4] Yi-Shan Lee,[5] Sheng-Di Lin,[6] Zhanghai Chen,[4] and Wei Xie[1,†]

[1]*State Key Laboratory of Precision Spectroscopy, School of Physics and Electronic Science, East China Normal University, Shanghai 200241, China*

[2]*Department of Physics and Astronomy, Michigan State University, Michigan 48824, USA*

[3]*School of Physics and Astronomy, and Tsung-Dao Lee Institute, Shanghai Jiao Tong University, Shanghai 200240, China*

[4]*State Key Laboratory of Surface Physics and Department of Physics, Fudan University, Shanghai 200433, China*

[5]*Department of Electrical Engineering, National Central University, Taoyuan 32001, Taiwan*

[6]*Department of Electronics Engineering, National Chiao Tung University, Hsinchu 30010, Taiwan*

[7]*Collaborative Innovation Center of Extreme Optics, Shanxi University, Shanxi 030006, China*

[8]*Shanghai Research Center for Quantum Sciences, Shanghai 201315, China*

(Received 6 June 2019; revised manuscript received 6 August 2019; accepted 19 March 2020; published 16 April 2020)

Macroscopic coherence of Bose condensates is a fundamental and practical phenomenon in many-body systems, such as the long-range correlation of exciton-polariton condensates with a dipole density typically below the exciton Mott-transition limit. Here we extend the macroscopic coherence of electron-hole-photon interacting systems to a new region in the phase diagram—the high-density plasma region, where long-range correlation is generally assumed to be broken due to the rapid dephasing. Nonetheless, a cooperative state of electron-hole plasma does emerge through the sharing of the superfluorescence field in an optical microcavity. In addition to the *in situ* coherence of *e-h* plasma, a long-range correlation is formed between two 8-μm-spaced plasma ensembles even at room temperature. Quantized and self-modulated correlation modes are generated for *e-h* ensembles in the plasma region. By controlling the distance between the two ensembles, multiple coupling regimes are revealed, from strong correlation to perturbative phase correlation and finally to an incoherent classical case, which has potential implications for tunable and high-temperature-compatible quantum devices.

DOI: 10.1103/PhysRevLett.124.157402

Bosons—photons, partial atoms, electron-hole dipoles, and other particles with integral spin quantum numbers—can condensate into a common quantum state by satisfying the critical conditions [1–6]. Recently, there is a new challenging frontier to investigate: the novel correlations between and among condensate ensembles in solid states. On the one hand, a condensate acting as a "large quasiparticle," could correlate with others to develop a superstrong interaction because of its large coupling strength and long coherence length [7–9]. On the other hand, the ability to control multiple quantum ensembles with high spatial and temporal sensitivity will stimulate advanced manipulation technologies for microintegrated devices [10,11]. In semiconductor microcavities [12,13], macroscopic quantum behaviors are revealed based on coherent polariton waves with a small dissipation rate and a large spreading velocity [9,10,14–17]. Although condensation actions have attracted continuing interest, with experimental discoveries even extending to surface plasma condensates [18] and magneto-optic quantum fluids [19–22], the phenomenon reported here has never been observed. Namely, a robust and room-temperature phase correlation is formed between two cooperative *e-h* plasma ensembles. we demonstrate the transregional coherence of *e-h* dipoles in the plasma region.

Macroscopic coherence could spontaneously appear from an incoherent *e-h* gas through the superfluorescence (SF) effect [23–25]. Here, in addition to the *in situ* coherence of *e-h* dipoles within the excitation area [26,27], the focus is on the establishment of phase correlation between two transregional ensembles. By introducing two cooperative plasmas into an optical microcavity, the coupling strength of two ensembles is dramatically enhanced due to the sharing of cavity-confined SF fields, which overcomes the dipole dephasing even at room temperature. Such a controllable correlation can find application in high-temperature quantum microdevices.

Figure 1(a) shows the sketch of sample structure. The GaAs/AlAs distributed Bragg reflector microcavity has three stacks of InGaAs/GaAs quantum wells (QWs), embedded at the antinodes of the cavity light field [28] (Supplemental Material [29], part I). Unlike the traditional planar microcavity system, the optical cavity resonance (E_c) here is detuned to ~80 meV above the QW band gap E_g' [Fig. 1(b)], which will suppress the radiative recombination of *e-h* pairs

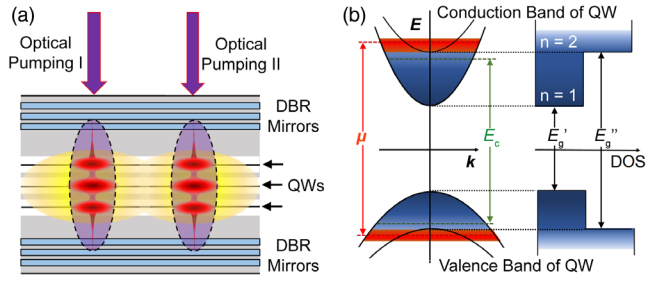

FIG. 1. (a) Microcavity structure. (b) Energy diagram. The bare cavity resonance E_c is 80 meV higher than the QW band gap E_g', and approaches to E_g''. Under intense excitation, the quasi-Fermi level μ of e-h plasma is beyond E_g''.

at the band gap and favor the accumulation of carriers. The excited state E_g'' for the transition $e2$-$hh2$ in QW is slightly beyond E_c ($E_g'' - E_c \approx 10$ meV). For the energy level above E_g'', the density of states (DOS) becomes higher [Fig. 1(b) and Fig. S2]. The sample is excited by a large-detuned 2 ps pulsed laser at energy of 1.58 eV at room temperature and high-density plasma is produced. Before investigating the transregional correlation of two e-h ensembles, the cooperative many-body state in a plasma gas is studied. It has been reported that a collective state could form near the Fermi edge of the high-density e-h plasma in bare QWs without packing cavity and SF has been observed at low temperature and high magnetic condition [26,27]. Here, we demonstrate that a fraction of e-h dipoles near the quasi-Fermi level (μ) of a plasma ensemble would form a cooperative e-h plasma state ($cehp$) and develop a phase correlation by coupling with the radiation field in a microcavity at room temperature.

The radiation behavior of cooperative plasma is studied by angle-resolved PL spectrum measurements [Figs. 2(a)–2(c)]. When the excitation density is below a critical density $P_{\rm th}$ (carrier density is $\sim 5 \times 10^{12}$ cm^{-2} per QW per pulse), weak optical signals radiate from the microcavity sample. The energy-momentum dispersion of the cavity mode is observed at ~1.40 eV. We have checked the carrier-induced shift of E_c, which is only several mega-electron volts (Supplemental Material [29], part III). As the density reaches the threshold $P_{\rm th}$, a narrow peak emerges at 1.42 eV, which is ~20 meV higher than E_c. This new peak is nondispersive, totally differing from the parabolic cavity mode. Moreover, its radiation behavior shows typical SF characteristics. The dynamics of PL signals are investigated at different excitation densities [Fig. 2(g)]. As the density increases, the PL radiation time $t_{\rm SF}$ rapidly decreases [Fig. 2(h)], while the peak intensity $I_{\rm max}$ of the time-dependent PL signal rises nonlinearly [Fig. 2(i)], in accordance with calculations based on the SF-cavity model [see the fitting curves in Figs. 2(h), 2(i) and Supplemental Material [29], part V]. Here, the SF signal is rooted in the $cehp$ state, and the threshold $P_{\rm th}$ is defined as the critical density of e-h dipoles above which the cavity-enhanced SF effect occurs.

Note that the $cehp$ state does not emerge at the cavity resonance E_c. By increasing the density of e-h dipoles, the quasi-Fermi level μ is raised, as seen in the PL spectra in Fig. S2 from the bare QW sample. For the e-h dipoles in QWs, the DOS at energy level equivalent to E_c or E_g' is demonstrated not high enough to induce the SF effect and to synchronize the phases of dipole moments in e-h ensemble. However, when μ rises above E_g'' [Fig. 2(c)], the higher DOS (at the order of 10^{11} meV^{-1} cm^{-2}) favors the formation of the $cehp$ state in the microcavity sample, accompanied by the SF signals [27]. Interestingly, the $cehp$ state does not form at the states far below μ, but shifts with the dynamical μ, shown as the dynamical evolution of the $cehp$ state during the radiative loss process of the ensemble

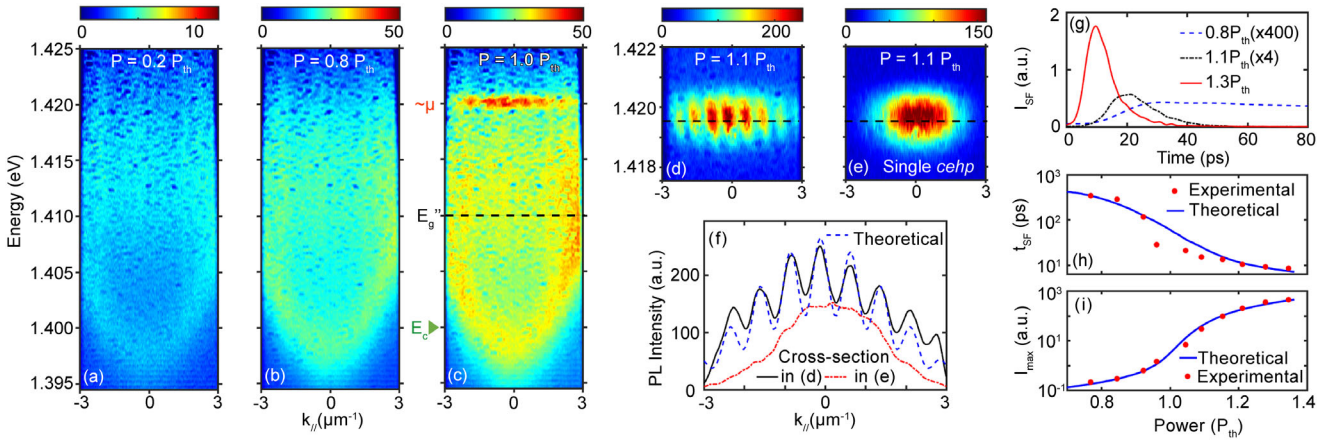

FIG. 2. (a)–(d) k-space PL spectra at different excitation densities obtained by double-beam excitation. The corresponding contrast spectrum under single-beam excitation is shown in (e). (f) Cross sections obtained from the black dashed lines in (d) and (e) and the theoretical fitting. (g)–(i) Visualized SF characteristics. PL dynamics are shown in (g), where the intensity is spectrally integrated. When increasing the pumping power, the radiative time $t_{\rm SF}$ of PL rapidly decreases (g),(h), while the peak PL intensity $I_{\rm max}$ rises nonlinearly (g),(i), in accordance with calculations based on the SF-cavity model.

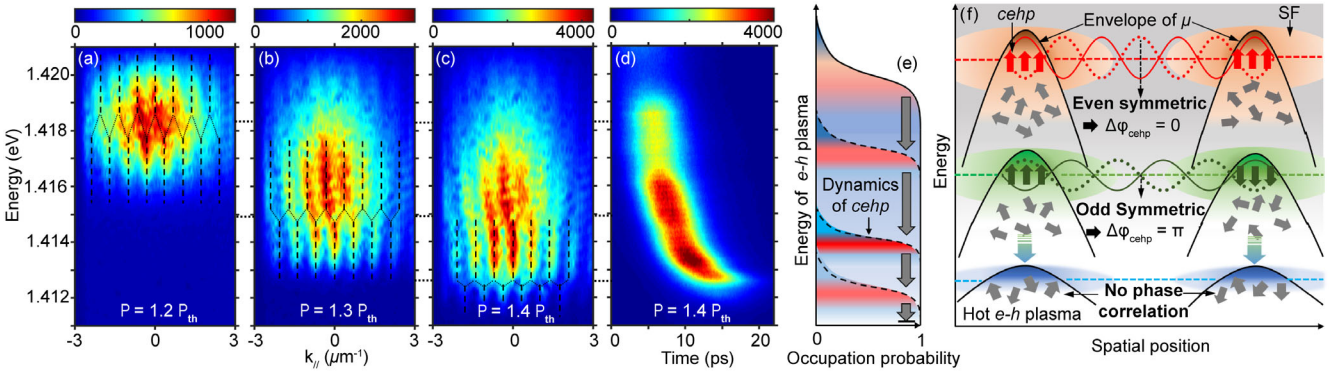

FIG. 3. (a)–(c) k-space spectra of two 8-μm-spaced $cehp$ states under different excitation densities. The central bright or dark fringe indicates the locked phase between two $cehp$ states $\Delta\varphi_{cehp}$ to be $0/\pi$. The black dashed lines are guidelines. (d) Time-resolved PL spectrum. (e) Evolution of the $cehp$ state, coordinating with the radiation process in (d). Four fragments are shown to sketch the e-h filling status of μ at different radiation moments. The red region represents the dipole component in a collective phase. The deeper coloring means better in-phase order in the dipole ensemble. (f) Sketches of generating a quantized phase correlation. The spatial-dependent μ envelopes represent the distribution of the e-h plasma excited by the Gaussian-distributed pumping beam. We ignore the temperature-induced broadening of carrier distribution along the energy axis for simplification. The arrows within the envelopes represent the phases of dipole moments.

[Figs. 3(d), 3(e)]. Thanks to the half-full and half-empty filling character of states near μ, on the one hand, there are sufficient dipole moments excited. On the other hand, the radiative dissipation process of dipole moments will be rarely affected by the incoherent refilling promoted by the upper energy states. The transition dipole moments could coherently couple with the mutual optical field [27,28,30]. Conversely, for the fully filled states below μ, the coherence time of the dipole moment becomes much shorter. The population of these states is dominated by incoherent state filling, rather than coherent interaction between the dipoles and optical field. Thus, the $cehp$ state, originating from in-phase organization of dipole moments assisted by a common light field, will not emerge at the states far below μ. The formation and the energy level of the $cehp$ state could also be revealed by the transient differential reflectance spectra in pump-probe measurements (Fig. S3 [29]). For the radiative e-h plasma in a cavity system [31–33], the long-range light field will enhance the dipole-dipole correlation and make it overcome the dipole dephasing mainly caused by the short-range scattering. As a result, a transient $cehp$ state with picosecond lifetime could exist even at room temperature in the microcavity.

Next, we focus on the transregional correlation between two cooperative plasma ensembles. When two $cehp$ droplets are simultaneously introduced without spatial overlap, the initially unrelated droplets may form a subtle phase correlation through the exchange of the in-plane components of the SF field. Such phase correlation is demonstrated by the k-space interference of the emissions from two $cehp$ droplets (Fig. S1 [29]). Experimentally, two $cehp$ droplets are excited with the center distance $D \approx 8$ μm. As the excitation density increases to $1.1P_{\mathrm{th}}$, distinct interference fringes emerge at the energy level of the $cehp$ state [Figs. 2(a)–2(d)]. Note that the coherence of excited plasmas do not inherit from the pumping laser for the large detuning pumping. All of the PL interference fringes are obtained by averaging the repetitive measurement data. Thus, the result indicates a robust and identical phase correlation between the two droplets. The interference fringes are symmetrically distributed with the central bright fringe at $k_{\parallel} = 0$, indicating the phase difference between the two $cehp$ states $\Delta\varphi_{cehp} = 0$. The interval of fringes is related to the distance separating the two $cehp$ droplets, which could be theoretically simulated as seen in the blue curve in Fig. 2(f).

By further increasing the excitation density, the radiation intensity of $cehp$ states shows a nonlinear growth [Figs. 3(a)–3(c) and Fig. S4 of the Supplemental Material [29]]. Moreover, a broad PL peak is observed, originating from the time-accumulating measurement during the entire dynamic PL process. The quasi-Fermi level μ of the plasma and the energy of $cehp$ (E_{cehp}) decrease when the system releases energy via radiation [Fig. 3(e)], demonstrated by the time-resolved spectrum in Fig. 3(d). Hence, the longitudinal section of Fig. 3(c) from high to low energies corresponds to the moment of PL signals from early to late. The interference fringes exist over a large energy or time range [Fig. 3(c)], which suggests the phase correlation of $cehp$ droplets is not only dynamic with an ultrafast response rate, but also self-modulated to lock with the stable phase. Interestingly, a quantized phase correlation is observed, corresponding to a regular switching of $\Delta\varphi_{cehp}$ between 0 and π [Figs. 3(a)–3(c)]. Here, the two $cehp$ droplets can serve as the sources of optical SF fields, and transverse standing waves (SW) will be produced in the optical microcavity if the two sources are coherent with a stable phase shift [Fig. 3(f)]. Based on the experimental

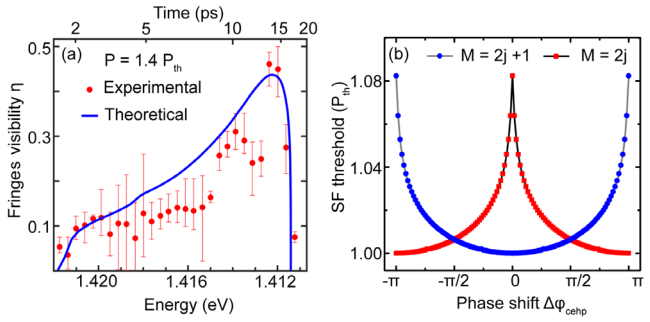

FIG. 4. (a) Energy-dependent visibility of interference fringes is extracted from Fig. 3(c). Here the error bars represent the inaccuracy of the visibility. (b) SF threshold of double-*cehp*-droplet system vs the locked phase of two *cehp* states $\Delta\varphi_{cehp}$ based on the theoretical simulation.

observations, there are two main conditions for *cehp*s to correlate efficiently: (i) Effective phase matching for constructive interference $\Delta\varphi_{cehp} + \Delta\varphi_{\mathrm{sw}} = 2j\pi$, where $\Delta\varphi_{\mathrm{sw}}$ is the additional phase of SW and $j \in N^{+}$, in which case the entire cavity system of the two *e-h* ensembles has the largest radiative rate and the lowest threshold to trigger the double-droplet SF effect (Fig. 4b). So when the order M of the activated SW mode is odd (even), the status of $\Delta\varphi_{cehp} = 0$ (or $\pm\pi$) will have the smallest threshold. Such a status has priority to obtain the stimulated amplification and dominates the system evolution. (ii) energy resonance condition $E_{cehp} \sim E_{\mathrm{sw}}$. After the distance of *cehp* droplets is fixed, the existing SW modes of discrete energies E_{sw} are determined (Fig. S10 [29]). During the SF process, E_{cehp} decreases, which induces a cascade activation of SW modes with the energy E_{sw} matching the real-time E_{cehp}. As a result, $\Delta\varphi_{cehp}$ will switch dynamically, the value of which depends on the symmetry of the SW mode coupling [Fig. 3(f)]. Based on the ultrafast optical channel and the short radiative time of SF, the phase correlation of *cehp*s can be achieved in a time order of a picosecond. Combining these features with the spatial manipulation technique of *e-h* ensembles, a quantized and miniature phase switch is realized with a response rate up to 0.2 THz. In addition, a redshift of the radiation range is observed when the excitation density is increased, which is related with the nonlinear characters of cavity *cehp* state (Fig. S4 [29]).

Furthermore, we extract the energy-dependent fringe visibility from Fig. 3(c) and plot it in Fig. 4(a). In the low-energy region of Figs. 3(c), 3(d), the *e-h* plasma exhibits low densities in the later period of PL radiation, and there is a low scattering rate between *cehp* and the reservoir carriers. Thus, high fringe visibility ($\eta \sim 0.5$) appears. Here, the coherence time of the *cehp*-photon hybrid field is dominated by the longitudinal relaxation time ($T_1 \sim 1$ ps, mainly determined by the cavity leakage rate of the optical component) instead of the transverse relaxation time (T_2, the purely dephasing time related to the *cehp*-carrier scattering in the material component). In contrast, the high-energy region of Figs. 3(c), 3(d) corresponds to the early stage of the SF process with a high *e-h* density. The scattering-induced dephasing of *cehp*

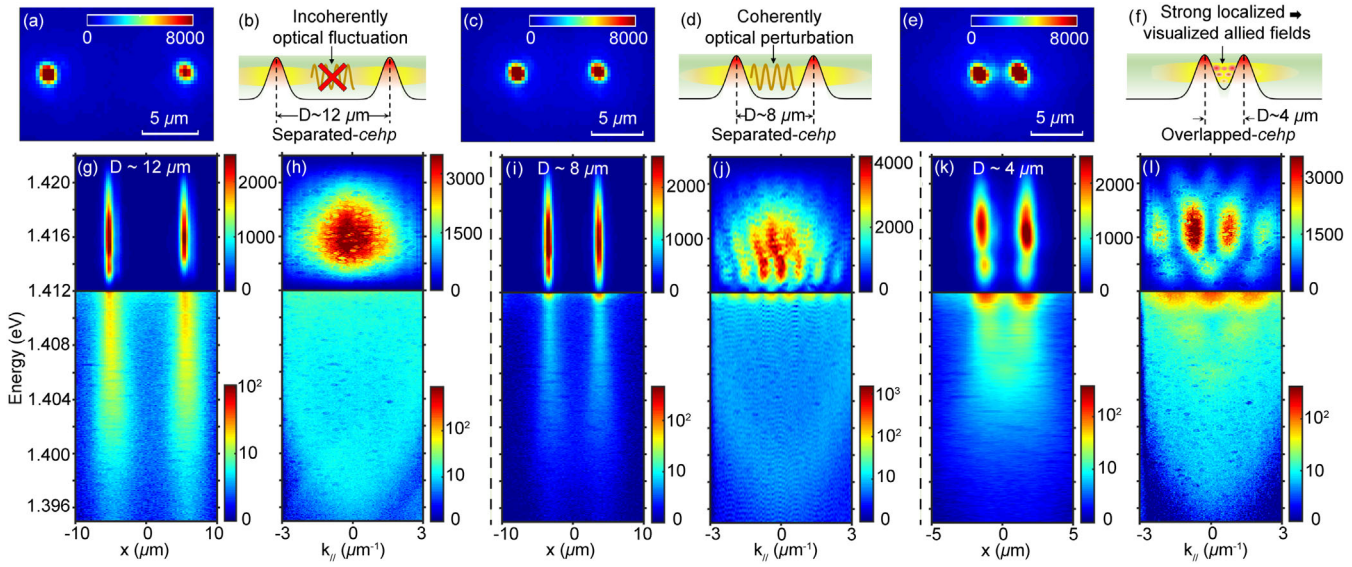

FIG. 5. (a),(c),(e) *r*-space PL images of *cehp* droplets at $P = 1.4P_{\mathrm{th}}$. (b),(d),(f) Key characteristics of different coupling regimes. (g)–(l) *r*-space and *k*-space spectra under three coupling regimes. Logarithmic color bar is used in the low-energy region for clarity. From left to right, due to the increase of coupling strength, the correlation of two *cehp* droplets is progressively enhanced, corresponding to the coupling regimes from "incoherent fluctuation in *r* space (b),(g) and linear superposition in *k* space (h)" to "coherent perturbation in *r* space (d),(i) and phase-correlation-induced interference in *k* space (j)," and "strong correlation of two overlapped *cehp* droplets in *r* space (e),(f) and visualized confined states of exchanging SF fields both in *r* and *k* spaces (k),(l)."

($T_2 \sim 0.2$ ps) yields a large energy linewidth ($\Delta E \sim \pm 2$ meV). Rare interference fringes can be observed in this case [Fig. 3(c) and Fig. 4(a)], revealing the upper limit of *e-h* carrier density ($\sim 10^{13}$ cm^{-2}) for long-range phase correlation.

By controlling the droplet distance, multiple coupling regimes are observed for the double-*cehp* system due to the tuning of coupling strength, i.e., the change of the allied SF field. In this sample, the attenuation length of the SF field is 5–10 μm. There is no clear interference fringe when the two *cehp* droplets are 12 μm apart [Figs. 5(a), 5(b), 5(g), 5(h)]. In contrast, the transregional coupling will be enhanced by decreasing the distance of the *cehp* droplets. Compared with the perturbative interaction of separated *cehp* droplets [Figs. 5(c), 5(d), 5(i), 5(j)], the overlapped *cehp* droplets could be strongly localized to the allied SF fields [Figs. 5(e), 5(f)], as seen in the visualized confined states of exchanging SF fields both in r-/k-space [Figs. 5(k), 5(l)]. For the perturbation case, the exchanging SF fields are weak. The emission signals from *cehp* droplets dominate the PL spectrum of Fig. 5(i). However, in the strongly localized case, obvious signals of exchanging SF fields are shown in Fig. 5(k). Accordingly, the distributions of confined SF fields are shown in the experimental data of Fig. 5(l) and in the theoretical simulation of Fig. S11 in the Supplemental Material [29]. The confinement potential of SF fields originates from the spatial overlap of the two Gaussian-distributed laser beams and the band filling of carriers in QWs [34,35].

In summary, in an electron-hole-photon interacting system, we extend the study of long-range coherence into the high-density, high-temperature region. A cooperative plasma state is observed near the quasi-Fermi energy level at room temperature. The setup process of transregional correlation between *cehp* droplets is transient and self-modulated by sharing their cavity-confined SF field. There are multiple coupling regimes for macroscopic coherence. We show the ability to control these novel quantum correlations in a double-plasma-ensemble system and to develop a quantized and miniature phase switch with high response rate. Our work will stimulate the studies of cooperative effects associated with spatial distributions and the development of ultrafast optoelectronic quantum devices at high temperature.

This Letter is supported by the National Key Research and Development Program of China under Grants No. 2016YFA0302001, No. 2018YFA0306304; the National Natural Science Foundation of China under Grants No. 11674097, No. 11654005, No. 91950201, No. 11234003, No. 11574086, No. 11974116, and No. 11674069; the Science and Technology Commission of Shanghai Municipality under Grant No. 16DZ2260200; Quantum Information Technology, Shanghai Municipal Science and Technology Major Project under Grant No. 2019SHZDZX01; the Fundamental Research Funds for the Central Universities; W. Z. also acknowledges additional support from the Shanghai talent program.

*wpz@sjtu.edu.cn
†wxie@phy.ecnu.edu.cn

[1] M. H. Anderson, J. R. Ensher, M. R. Matthews, C. E. Wieman, and E. A. Cornell, Science **269**, 198 (1995).
[2] K. B. Davis, M. O. Mewes, M. R. Andrews, N. J. van Druten, D. S. Durfee, D. M. Kurn, and W. Ketterle, Phys. Rev. Lett. **75**, 3969 (1995).
[3] J. Klaers, J. Schmitt, F. Vewinger, and M. Weitz, Nature (London) **468**, 545 (2010).
[4] A. A. High, J. R. Leonard, A. T. Hammack, M. M. Fogler, L. V. Butov, A. V. Kavokin, K. L. Campman, and A. C. Gossard, Nature (London) **483**, 584 (2012).
[5] A. Kogar, M. S. Rak, S. Vig, A. A. Husain, F. Flicker, Y. Joe, L. Venema, G. J. MacDougall, T. C. Chiang, E. Fradkin, J. Wezel, and P. Abbamonte, Science **358**, 1314 (2017).
[6] H. Deng, G. Weihs, C. Santori, J. Bloch, and Y. Yamamoto, Science **298**, 199 (2002).
[7] J. Kasprzak, M. Richard, S. Kundermann, A. Baas, P. Jeambrun, J. M. J. Keeling, F. M. Marchetti, M. H. Szymańska, R. André, J. L. Staehli, V. Savona, P. B. Littlewood, B. Deveaud, and Le Si Dang, Nature (London) **443**, 409 (2006).
[8] H. Deng, G. S. Solomon, R. Hey, K. H. Ploog, and Y. Yamamoto, Phys. Rev. Lett. **99**, 126403 (2007).
[9] L. Zhang, W. Xie, J. Wang, A. Poddubny, J. Lu, Y. Wang, J. Gu, W. Liu, D. Xu, X. Shen, Y. G. Rubo, B. L. Altshuler, A. V. Kavokin, and Z. Chen, Proc. Natl. Acad. Sci. U.S.A. **112**, E1516 (2015).
[10] C. W. Lai, N. Y. Kim, S. Utsunomiya, G. Roumpos, H. Deng, M. D. Fraser, T. Byrnes, P. Recher, N. Kumada, T. Fujisawa, and Y. Yamamoto, Nature (London) **450**, 529 (2007).
[11] E. Wertz, L. Ferrier, D. D. Solnyshkov, R. Johne, D. Sanvitto, A. Lemaître, I. Sagnes, R. Grousson, A. V. Kavokin, P. Senellart, G. Malpuech, and J. Bloch, Nat. Phys. **6**, 860 (2010).
[12] A. V. Kavokin, J. J. Baumberg, G. Malpuech, and L. P. Laussy, *Microcavities* (Oxford University Press, New York, 2017).
[13] H. Deng, G. Weihs, D. Snoke, J. Bloch, and Y. Yamamoto, Proc. Natl. Acad. Sci. U.S.A. **100**, 15318 (2003).
[14] K. G. Lagoudakis, M. Wouters, M. Richard, A. Baas, I. Carusotto, R. André, Le Si Dang, and B. Deveaud-Plédran, Nat. Phys. **4**, 706 (2008).
[15] A. Dreismann, P. Cristofolini, R. Balili, G. Christmann, F. Pinsker, N. G. Berloff, Z. Hatzopoulos, P. G. Savvidis, and J. J. Baumberg, Proc. Natl. Acad. Sci. U.S.A. **111**, 8770 (2014).
[16] Y. Sun, Y. Yoon, M. Steger, G. Liu, L. N. Pfeiffer, K. West, D. W. Snoke, and K. A. Nelson, Nat. Phys. **13**, 870 (2017).
[17] G. Lerario, A. Fieramosca, F. Barachati, D. Ballarini, K. S. Daskalakis, L. Dominici, M. D. Giorgi, S. A. Maier, G. Gigli, S. Kéna-Cohen, and D. Sanvitto, Nat. Phys. **13**, 837 (2017).

[18] T. K. Hakala, A. J. Moilanen, A. I. Väkeväinen, R. Guo, J. Martikainen, K. S. Daskalakis, H. T. Rekola, A. Julku, and P. Törmä, Nat. Phys. **14**, 739 (2018).
[19] S. O. Demokritov, V. E. Demidov, O. Dzyapko, G. A. Melkov, A. A. Serga, B. Hillebrands, and A. N. Slavin, Nature (London) **443**, 430 (2006).
[20] X. Li, M. Bamba, Q. Zhang, S. Fallahi, G. C. Gardner, W. Gao, M. Lou, K. Yoshioka, M. J. Manfra, and J. Kono, Nat. Photonics **12**, 324 (2018).
[21] D. A. Bozhko, A. A. Serga, P. Clausen, V. I. Vasyuchka, F. Heussner, G. A. Melkov, A. Pomyalov, V. S. L'vov, and B. Hillebrands, Nat. Phys. **12**, 1057 (2016).
[22] X. Li, M. Bamba, N. Yuan, Q. Zhang, Y. Zhao, M. Xiang, K. Xu, Z. Jin, W. Ren, G. Ma, S. Cao, D. Turchinovich, and J. Kono, Science **361**, 794 (2018).
[23] R. H. Dicke, Nat. Rev. **93**, 99 (1954).
[24] K. Cong, Q. Zhang, Y. Wang, G. T. Noe II, A. Belyanin, and J. Kono, J. Opt. Soc. Am. B **33**, C80 (2016).
[25] Y. D. Jho, X. Wang, D. H. Reitze, J. Kono, A. A. Belyanin, V. V. Kocharovsky, Vl. V. Kocharovsky, and G. S. Solomon, Phys. Rev. B **81**, 155314 (2010).
[26] G. T. Noe II, J. Kim, J. Lee, Y. Wang, A. K. Wójcik, S. A. McGill, D. H. Reitze, A. A. Belyanin, and J. Kono, Nat. Phys. **8**, 219 (2012).
[27] J. H. Kim, G. T. Noe II, S. A. McGill, Y. Wang, A. K. Wójcik, A. A. Belyanin, and J. Kono, Sci. Rep. **3**, 3283 (2013).
[28] F. K. Hsu, W. Xie, Y. S. Lee, S. D. Lin, and C. W. Lai, Phys. Rev. B **91**, 195312 (2015).
[29] See Supplemental Material at http://link.aps.org/supplemental/10.1103/PhysRevLett.124.157402 for supplementary evidences and discussions for the physics of the *cehp* states.
[30] J. Wagner, A. Ruiz, and K. Ploog, Phys. Rev. B **43**, 12134 (1991).
[31] P. R. Eastham and P. B. Littlewood, Phys. Rev. B **64**, 235101 (2001).
[32] M. Yamaguchi, K. Kamide, T. Ogawa, and Y. Yamamoto, New J. Phys. **14**, 065001 (2012).
[33] M. Yamaguchi, K. Kamide, R. Nii, T. Ogawa, and Y. Yamamoto, Phys. Rev. Lett. **111**, 026404 (2013).
[34] G. Tosi, G. Christmann, N. G. Berloff, P. Tsotsis, T. Gao, Z. Hatzopoulos, P. G. Savvidis, and J. J. Baumberg, Nat. Phys. **8**, 190 (2012).
[35] N. G. Berloff, M. Silva, K. Kalinin, A. Askitopoulos, J. D. Töpfer, P. Cilibrizzi, W. Langbein, and P. G. Lagoudakis, Nat. Mater. **16**, 1120 (2017).